THE JOURNAL OF PHYSICAL CHEMISTRY Letters

Cite This: J. Phys. Chem. Lett. 2019, 10, 2481−2486

Letter

pubs.acs.org/JPCL

Two-Dimensional Infrared Spectroscopy Reveals Molecular Self-Assembly on the Surface of Silver Nanoparticles

Anup Ghosh,[†] Amit K. Prasad,[†] and Lev Chuntonov*

Schulich Faculty of Chemistry and Solid State Institute, Technion − Israel Institute of Technology, Haifa 3200003, Israel

Supporting Information

ABSTRACT: The conformation of molecules, peptides, and proteins, self-assembled into structured monolayers on the surface of metal nanoparticles (NPs), can strongly affect their properties and use in chemical or nanobiomedical applications. Elucidating molecular conformations on the NP surface is highly challenging, and the microscopic details mostly remain elusive. Using polarization-selective third-order two-dimensional ultrafast infrared spectroscopy, we revealed the highly ordered intermolecular structure of γ-tripeptide glutathione on the surface of silver NPs in aqueous solution. Glutathione is an antioxidant thiol abundant in living cells; it is extensively used in NP chemistry and related research. We identified conditions where the interaction of glutathione with the NP surface facilitates formation of a β-sheet-like structure enclosing the NPs. A spectroscopic signature associated with the assembly of β-sheets into an amyloid fibril-like structure was also observed. Remarkably, the interaction with the metal surface promotes formation of a fibril-like structure by a small peptide involving only two amino acids.

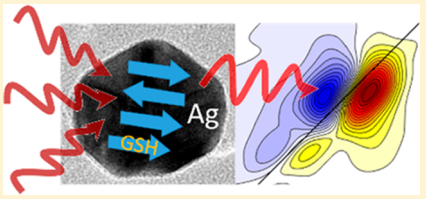

Functionalized nanomaterials have recently been the focus of extensive scientific research directed toward better understanding the interaction of their surfaces with (bio)-molecules.[1−4] Having a detailed understanding of factors affecting the self-assembly of molecules, peptides, and proteins on the surface of noble-metal nanoparticles (NPs) is important for numerous applications, including nano-optics,[5] biosensors,[6] heterogeneous catalysis,[7] NP-based drug delivery,[8,9] etc.[10,11] The microscopic structure of the self-assembled molecular monolayer (SAM) can have an enormous effect on the NP properties, for example, facilitating efficient cell membrane penetration.[12] Glutathione (GSH) is a tripeptide (γ-Glu-Cys-Gly) whose thiol group acts as an antioxidant in cells, where GSH is abundant; it is extensively used as a NP capping ligand.[13] The uptake of the GSH-protected NPs by cancer cells was found to be superior to NPs with mixed SAMs involving GSH molecules.[14,15] Small GSH-coated gold NPs were proposed as an efficient cell delivery system[16] and as amyloid fibril inhibiting agents.[11] Presumably, these special properties of the GSH-coated NPs stem from the multiple possibilities available for intermolecular hydrogen bonding in GSH, allowing for the formation of the organized capping layer by this ligand.[17−20]

A detailed structural characterization of intermolecular and molecule−NP surface interactions is needed to fully explore opportunities for the rational design of SAMs in NP applications;[21−23] however, achieving such a characterization is often challenging.[23−27] GSH monolayers on gold surfaces were extensively studied by various methods.[28−33] It was revealed that in aqueous solutions GSH attaches to the metal via the cysteine, and that at a pH range of 4−9, it appears in anionic (Gly) and zwitterionic (Glu) forms.[19,20,28−33] However, despite the extensive investigations, a detailed microscopic picture of the GSH SAM structure has remained elusive. Herein, we meet this challenge by applying a full arsenal of two-dimensional ultrafast infrared spectroscopy (2DIR) tools.[34−37] In 2DIR, the spectrum is spread in two dimensions allowing for separation of the line shape components and resolving molecular conformations with congested spectra. The cross-peaks indicate the coupling between the vibrational modes and the associated transfer of the vibrational excitation.[38−40]

In studies of biomolecules, infrared spectroscopy of amide carbonyl stretching vibrational mode (amide-I) is particularly informative.[41] Indeed, 2DIR spectroscopy of free GSH in solution indicates coupling between its two amide-I modes with the corresponding cross-peaks, facilitating their assignment. On the other hand, GSH SAMs on the NP surface reveals spectroscopic signatures of the molecular organization, typical of the β-sheets formed in proteins and peptides.[41−44] Here, the coupling between multiple amide-I modes of the amino acids comprising the β-sheet results in the appearance of a collective delocalized exciton mode, red-shifted from their individual transitions.[45,46] Recently, Lomont et al.[47] found that in contrast to β-sheet-rich oligomers, when amyloid fibrils are formed, stronger coupling between the amide-I modes leads to the emergence of an additional red-shifted transition. Similar signatures were observed in our experiments, suggesting that GSH SAM is organized in β-sheet-like and fibril-like structures.

The GSH molecules were self-assembled on the surface of the 40 nm silver NPs;[48] the pH of the solution was 5.5. Linear absorption of the amide-I mode of free GSH in D_2O (Figure 1A) shows several overlapping broadband transitions. 2DIR

Received: February 24, 2019
Accepted: April 12, 2019
Published: April 12, 2019

DOI: 10.1021/acs.jpclett.9b00530
J. Phys. Chem. Lett. 2019, 10, 2481−2486

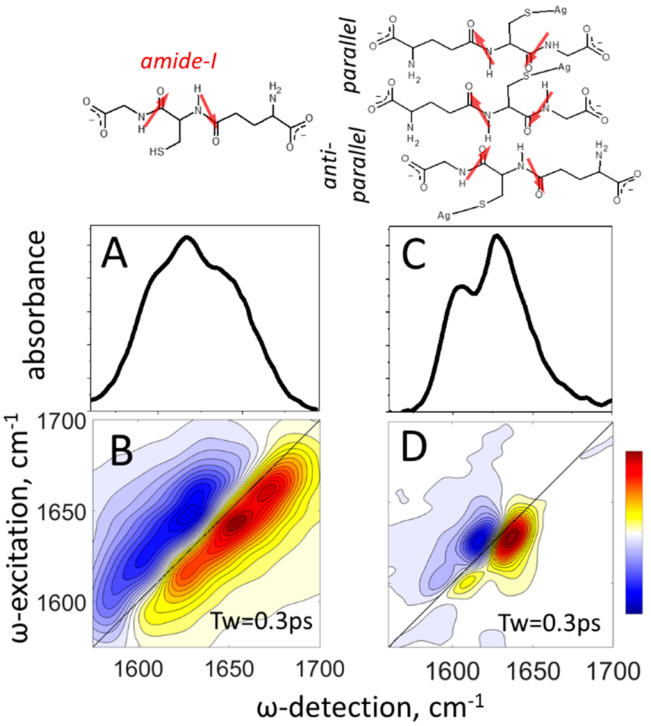

Figure 1. Infrared spectroscopy of GSH. Linear absorption (A) and 2DIR spectrum (B) of a 0.1 M solution of free GSH in D_2O, pD 5.5. Linear absorption (C) and 2DIR spectrum (D) of SAM GSH on the surface of 40 nm silver NPs. GSH molecules are illustrated above with the transition dipole moments of the amide-I modes indicated by red arrows. Both parallel and antiparallel β-sheet-like conformations are illustrated; see text for discussion.

spectroscopy (Figure 1B) resolves the congested spectra into four peaks assigned to amide-I transitions in Cys and Gly (ω_{ex} = 1665 and 1645 cm^{-1}) and to the antisymmetric stretching of the deprotonated carboxylic groups of the Glu and Gly units (ω_{ex} = 1618 and 1595 cm^{-1}).[29,49] This assignment is supported by the ability of the polarization-selective 2DIR to identify the intermode coupling.[38,39] A series of waiting time (T_w)-dependent spectra recorded for pD values of 2, 5.5, and 12 are shown in Figure 2. For the all-parallel polarization of the excitation pulses, ⟨XXXX⟩, the cross-peak between the coupled amide-I modes is not seen clearly at T_w = 0.3 ps; however, it becomes noticeable at T_w = 1.5 ps. For the cross-polarized pulse sequence, ⟨YYXX⟩, the cross-peak becomes clearly visible at ω_{ex} = 1645 cm^{-1}; ω_{det} = 1670 cm^{-1}, especially at T_w = 1.5 ps.[39] This trend was observed for all pD values. At low pD values, both carboxyl groups in glutathione are protonated (pK_a = 2 and 3.4 for Glu and Gly, respectively), and the carboxylic stretching transitions appear at ω_{ex} = 1730 cm^{-1}. This transition is gradually replaced by bands at ω_{ex} = 1618 and 1595 cm^{-1} when the pD value rises; the latter is especially intensified after the deprotonation of the amine on the Glu unit (pK_a = 9.5), as seen in Figure 2.[29] Finally, the cross-peak at ω_{ex} = 1618 cm^{-1}; ω_{det} = 1675 cm^{-1} suggests mode connectivity because of the short intramolecular distance between the carboxylic stretching and the amide-I modes of Gly.[50,51]

In contrast to the free GSH, the linear spectrum of GSH SAM (Figure 1C) shows two narrowed transitions at ω_{ex} = 1628 and 1604 cm^{-1}. The former is the well-known marker of the vibrational exciton of β-sheets,[45,52,53] whereas the latter suggests a fibril-like structure.[47] The corresponding 2DIR spectrum in Figure 1D remarkably resembles that of the amyloid fibrils in ref 47. To quantitatively analyze the spectrum we fitted the linear spectrum of the SAM GSH and the diagonal slice of its 2DIR spectrum to two peaks, as shown in Figure S2. Assuming similar strengths of the transition dipole moments of the β-sheet-like and fibril-like structures, the ratio

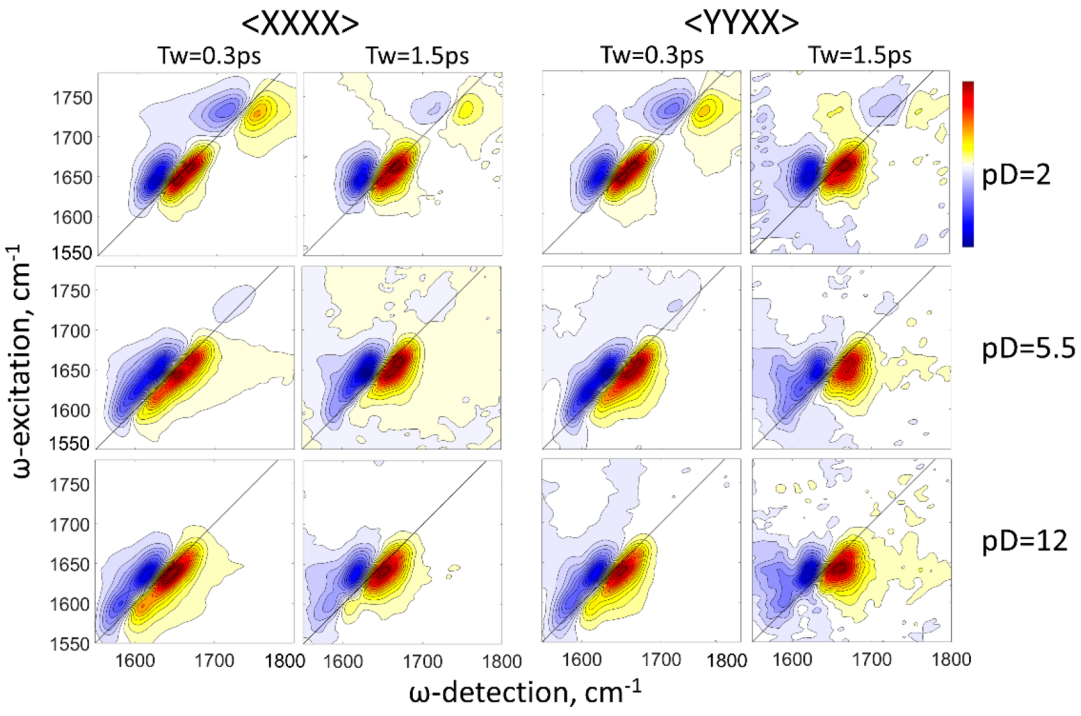

Figure 2. Polarization-selective 2DIR spectroscopy of free GSH. The polarization of the excitation pulses and the waiting times corresponding to the spectra in each column are indicated at the top. The pD values for each row appear on the right.

DOI: 10.1021/acs.jpclett.9b00530
J. Phys. Chem. Lett. 2019, 10, 2481−2486

of the peak areas for both linear and 2DIR spectra represents the ratio of the concentrations of the two conformations. We obtained that ca. 15% of the sample adopts fibril-like conformation, as compared to the 25% reported in ref 47 for amyloid peptides.

Reduction in both the inhomogeneous and the homogeneous line width of the SAM GSH, as compared to the free GSH, is reflected in the diagonal and the antidiagonal width of the 2DIR peak, respectively. The line narrowing is consistent with the formation of the ordered intermolecular structure constrained to the NP surface.[23,54] Narrower line shapes generally indicate slower molecular dynamics. The correlation function of the frequency fluctuations (FFCF), reflecting SAMs' ultrafast dynamics, decays slower, compared with that of free molecules in solution.[55,56] For a single-oscillator transition, the T_w-dependence of the nodal line slope (NLS) of the 2D peak serves as a measure of the spectral diffusion.[57] In the cases of coupled vibrational modes (free GSH) and excitonic transitions (GSH SAM), equilibration of the excitation between the coupled modes can scramble the NLS signature of the FFCF decay. However, even though the NLSs in our data cannot be strictly associated with the FFCF, it can still serve as a parameter qualitatively describing the very different spectral evolution observed in the free GSH and GSH SAM.[58,59]

The evolution of the NLS for free and SAM GSH evaluated at the lower amide-I transition frequency is compared in Figure 3. The NLS of the free GSH signal decays exponentially (τ = 0.35 ± 0.1 ps) to an offset amplitude representing static inhomogeneity of the transition. Note that this decay is significantly faster than the population transfer between the coupled amide-I modes leading to growth of the cross-peaks in Figure 2.[40] On the other hand, the NLS of SAM GSH appears as a straight line on the experimental time scale (limited by the vibrational relaxation of the amide-I mode). Although its decay is so slow that the time constant cannot be estimated, it is clear that the static inhomogeneity is smaller for the SAM GSH.[60] The lower initial value of the NLS of SAM GSH, compared to that of free GSH, indicates a larger relative contribution of the homogeneous component to the total line width. However, the static inhomogeneity is smaller, the overall width is reduced, and the slowing of the T_w-dependent dynamics of the SAM GSH transition is evident. These observations suggest a highly ordered molecular structure of the SAM GSH.

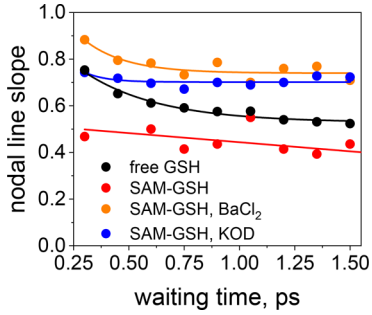

Figure 3. Spectral diffusion of GSH. Circles, experimental values of the nodal line slope; lines, their fit to the data. Black, free GSH molecules, pD 5.5; red, SAM GSH; orange, SAM GSH with $BaCl_2$ added to the sample, pD 3.5; blue, SAM GSH with KOD added to the sample, pD 12.

In the pD 5.5 solutions of free GSH, the signal associated with the protonated fraction of the carboxylic groups is not observed. Regarding SAM GSH, the corresponding transition appears 6 times weaker than that of the amide-I band in the linear spectrum (Figure S3) and 40 times weaker in 2DIR. The presence of this transition provides interesting information on the GSH SAM structure. Because the pK_a value of Gly carboxyl is higher than that of Glu, it is more prone to protonation, for example, by the Glu amine of the neighboring strand, available for hydrogen bonding in the β-sheet arrangement. At the same time, in contrast to free GSH, no transition associated with the anionic carboxyl groups is seen for GSH SAM. This can be rationalized by the sensitivity of the SAM conformation to the silver surface charge. At high pD values, the surface of the silver NPs[61] is negatively charged by the adsorbed hydroxyl anions, whereas at low pD values the surface charge is positive, and the point-of-zero-charge is at pD 7, as estimated by Merga et al.[62] Thus, at pD 5.5 the carboxyl anions are prone to interact with surface cations. This interaction leads to elimination of the carboxyl stretching transition from the spectral region monitored in our experiment either because of the strong deformation of the electronic potential, leading to a dramatic shift of the transition frequency, or because of the orientation of the transition dipole parallel to the surface and manifestation of the surface selection rules.[63]

In order to test the sensitivity of the β-sheet conformation to the solvation environment, we added to the GSH-capped NP solution either metal ions ($BaCl_2$) or alkali base (KOD). Barium ions compete with the positively charged NP surface, because they are chelated by the carboxylic anions,[28] leading to a conformational change in GSH SAM and disruption of β-sheets.[64] The corresponding spectra in Figure 4A,B show

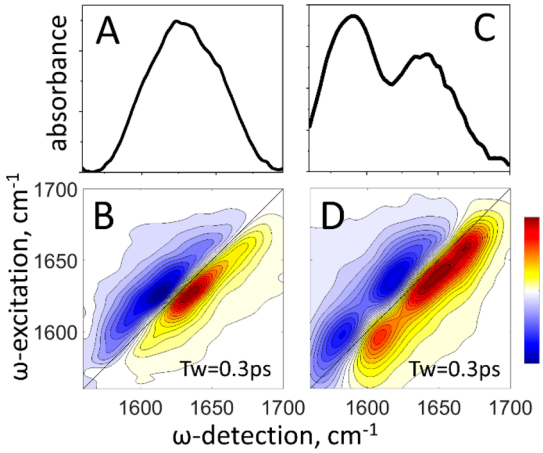

Figure 4. Infrared spectroscopy of disrupted GSH SAM. Linear spectroscopy (A) and 2DIR (B) of GSH SAM on the NP surface, when $BaCl_2$ was added into the solution. Linear spectroscopy (C) and 2DIR of GSH SAM on the NP surface, when KOD was added into the solution.

transitions at ω_{ex} = 1665 and 1645 cm^{-1}, similar to those of free GSH at low pD values. Analysis of the NLS of the amide-I transition (Figure 3) shows that FFCF decays at a rate similar to that of free GSH (τ = 0.24 ± 0.12 ps); however, the contribution of the homogeneous component to the line shape is smaller and the inhomogeneity increases. Subsequently, deuteryl anions disrupt β-sheets by passivating the NPs, which leads to the carboxyl groups repulsing from the surface. The

DOI: 10.1021/acs.jpclett.9b00530
J. Phys. Chem. Lett. 2019, 10, 2481−2486

corresponding spectra in Figure 4C,D resemble those observed for solutions of free GSH at high pD values, with emphasized transition at ω_{ex} = 1595 cm^{-1}. Analysis of the NLS (Figure 3) indicates that also here static inhomogeneity exceeds that of free GSH.

Recently, Mandal et al.[65] observed that leucine-rich peptide, fully helical in solution, assembles into an antiparallel β-sheet on the surface of 5 nm NPs (ω_{ex} = 1625 cm^{-1}) but not on the surface of larger 20 nm NPs and on flat surfaces. In contrast, Shaw et al.[54] observed that the fraction of the parallel β-sheet formed by the amyloid-derived peptide (ω_{ex} = 1665 and 1640 cm^{-1}) increased with NP size. Our own results for GSH SAM on the surface of 2 nm silver NPs[66] indicate that β-sheets are not formed and that the corresponding spectra (Figures S3 and S5) qualitatively resemble those of free GSH at pD 5.5, illustrating the critical role of surface flatness in promoting the formation of GSH β-sheets. Di Gregorio et al.[67] noted that chiroptical signal of the GSH-capped silver nanocubes vanishes upon raising the pH. Indeed, in our samples we observed that the β-sheet's circular dichroism, a positive transition at 203 nm, disappears upon addition of the barium or deuteryl ions (Figure S6), confirming disruption of β-sheets.

In 2DIR spectroscopy, the parallel and antiparallel β-sheets are distinguished by the cross-peaks appearing in the latter case.[45,46,52,68] On metal NPs, the electromagnetic boundary conditions require that direction of the electric field is normal to the surface[69,70] and surface selection rules are implied.[63] The low-frequency amide-I exciton mode of the β-sheet has transition dipole moment perpendicular to the strand axis.[71] For the parallel β-sheet, the transition dipole is inclined to the plane of the sheet, such that if the sheet lies parallel to the metal surface, its out-of-plane component would survive the selection rules. On the other hand, for the antiparallel β-sheet, the corresponding transition dipole moment is in-plane with the sheet[71] and would not be observed. The weaker high-frequency exciton mode of the antiparallel β-sheets has transition dipole moment parallel to the strand, in-plane with the sheet.[71] Thus, any signal from the antiparallel β-sheet whose plane is parallel to the NP surface would vanish. Interestingly, we have not detected high-frequency transition associated with the antiparallel beta-sheet nor the corresponding cross-peaks in the polarization-selective measurements of SAM GSH (Figure S4), suggesting that if any antiparallel β-sheet SAM is formed, its plane is parallel to the NP surface and it is not observed in our measurements. Therefore, the signal reported in the present work represents the parallel β-sheet SAM. Interestingly, it is in contrast to conclusions of NMR studies of the oxidized disulfide GSH dimer, self-assembled into gels, where antiparallel β-sheets are stabilized by the restricted rotation about the disulfide bond.[17]

In conclusion, using polarization-selective 2DIR spectroscopy, we revealed molecular conformations of GSH on the surface of silver NPs. The thiol−silver bonds and the interaction of the carboxylic anions with silver surface cations facilitate formation of the β-sheet-like and fibril-like structures enclosing the NP. Remarkably, the fibril-like structure is formed by a small peptide with only two amino acids. A weak, yet visible signal of the protonated carboxyl is also seen, when β-sheets are formed. The conformation of the β-sheet appears predominantly parallel; however, we cannot rule out the presence of the antiparallel β-sheets, whose plane is parallel to the NP surface. The structural response of β-sheets to a change in the environment is important not only for the chemical and nanotechnological applications of the GSH-capped NPs but also for NP-based medicine, because GSH is abundant in the cytosol and can potentially exchange with various NP ligands. Internalized NPs with GSH SAM eventually reach the acidic lysosome, where the fibril-like structure on their surface may initiate various processes.[72]

■ ASSOCIATED CONTENT

Supporting Information

The Supporting Information is available free of charge on the ACS Publications website at DOI: 10.1021/acs.jpclett.9b00530.

Experimental methods and additional experimental results (PDF)

■ AUTHOR INFORMATION

Corresponding Author

*E-mail: chunt@technion.ac.il.

ORCID

Lev Chuntonov: 0000-0002-2316-4708

Author Contributions

†A.G. and A.K.P. contributed equally to this work.

Notes

The authors declare no competing financial interest.

■ ACKNOWLEDGMENTS

This research is supported by the Israel Science Foundation (grant 1118/15) and the Russell Berrie Nanotechnology Institute, Technion.

■ REFERENCES

(1) Sapsford, K. E.; Algar, W. R.; Berti, L.; Gemmill, K. B.; Casey, B. J.; Oh, E.; Stewart, M. H.; Medintz, I. L. Functionalizing Nanoparticles with Biological Molecules: Developing Chemistries That Facilitate Nanotechnology. *Chem. Rev.* **2013**, *113*, 1904−2074.

(2) Nel, A. E.; Mädler, L.; Velegol, D.; Xia, T.; Hoek, E. M. V.; Somasundaran, P.; Klaessig, F.; Castranova, V.; Thompson, M. Understanding Biophysicochemical Interactions at the Nano−Bio Interface. *Nat. Mater.* **2009**, *8*, 543.

(3) Vallee, A.; Humblot, V.; Pradier, C.-M. Peptide Interactions with Metal and Oxide Surfaces. *Acc. Chem. Res.* **2010**, *43*, 1297−1306.

(4) Slocik, J. M.; Naik, R. R. Probing Peptide−Nanomaterial Interactions. *Chem. Soc. Rev.* **2010**, *39*, 3454−3463.

(5) Haran, G.; Chuntonov, L. Artificial Plasmonic Molecules and Their Interaction with Real Molecules. *Chem. Rev.* **2018**, *118*, 5539−5580.

(6) Howes, P. D.; Chandrawati, R.; Stevens, M. M. Colloidal Nanoparticles as Advanced Biological Sensors. *Science* **2014**, *346*, 1247390.

(7) Mikolajczak, D. J.; Koksch, B. Peptide-Gold Nanoparticle Conjugates as Sequential Cascade Catalysts. *ChemCatChem* **2018**, *10*, 4324−4328.

(8) Han, G.; Ghosh, P.; Rotello, V. M. Functionalized Gold Nanoparticles for Drug Delivery. *Nanomedicine* **2007**, *2*, 113−123.

(9) Dykman, L. A.; Khlebtsov, N. G. Uptake of Engineered Gold Nanoparticles into Mammalian Cells. *Chem. Rev.* **2014**, *114*, 1258−1288.

(10) Gladytz, A.; Abel, B.; Risselada, H. J. Gold-Induced Fibril Growth: The Mechanism of Surface-Facilitated Amyloid Aggregation. *Angew. Chem., Int. Ed.* **2016**, *55*, 11242−11246.

(11) Gao, G.; Zhang, M.; Gong, D.; Chen, R.; Hu, X.; Sun, T. The Size-Effect of Gold Nanoparticles and Nanoclusters in the Inhibition of Amyloid-B Fibrillation. *Nanoscale* **2017**, *9*, 4107−4113.

DOI: 10.1021/acs.jpclett.9b00530
J. Phys. Chem. Lett. 2019, 10, 2481−2486

(12) Pengo, P.; Şologan, M.; Pasquato, L.; Guida, F.; Pacor, S.; Tossi, A.; Stellacci, F.; Marson, D.; Boccardo, S.; Pricl, S.; Posocco, P. Gold Nanoparticles with Patterned Surface Monolayers for Nanomedicine: Current Perspectives. *Eur. Biophys. J.* **2017**, *46*, 749−771.
(13) Hong, R.; Han, G.; Fernández, J. M.; Kim, B.-j.; Forbes, N. S.; Rotello, V. M. Glutathione-Mediated Delivery and Release Using Monolayer Protected Nanoparticle Carriers. *J. Am. Chem. Soc.* **2006**, *128*, 1078−1079.
(14) Lund, T.; Callaghan, M. F.; Williams, P.; Turmaine, M.; Bachmann, C.; Rademacher, T.; Roitt, I. M.; Bayford, R. The Influence of Ligand Organization on the Rate of Uptake of Gold Nanoparticles by Colorectal Cancer Cells. *Biomaterials* **2011**, *32*, 9776−9784.
(15) Amarnath, K.; Mathew, N. L.; Nellore, J.; Siddarth, C. R. V.; Kumar, J. Facile Synthesis of Biocompatible Gold Nanoparticles from Vites Vinefera and Its Cellular Internalization against Hbl-100 Cells. *Cancer Nanotechnol.* **2011**, *2*, 121−132.
(16) Sousa, A. A.; Morgan, J. T.; Brown, P. H.; Adams, A.; Jayasekara, M. S.; Zhang, G.; Ackerson, C. J.; Kruhlak, M. J.; Leapman, R. D. Synthesis, Characterization, and Direct Intracellular Imaging of Ultrasmall and Uniform Glutathione-Coated Gold Nanoparticles. *Small* **2012**, *8*, 2277−2286.
(17) Lyon, R. P.; Atkins, W. M. Self-Assembly and Gelation of Oxidized Glutathione in Organic Solvents. *J. Am. Chem. Soc.* **2001**, *123*, 4408−4413.
(18) Matsuura, K.; Matsuyama, H.; Fukuda, T.; Teramoto, T.; Watanabe, K.; Murasato, K.; Kimizuka, N. Spontaneous Self-Assembly of Nanospheres from Trigonal Conjugate of Glutathione in Water. *Soft Matter* **2009**, *5*, 2463−2470.
(19) Lim, I.-I. S.; Mott, D.; Ip, W.; Njoki, P. N.; Pan, Y.; Zhou, S.; Zhong, C.-J. Interparticle Interactions in Glutathione Mediated Assembly of Gold Nanoparticles. *Langmuir* **2008**, *24*, 8857−8863.
(20) Moaseri, E.; Bollinger, J. A.; Changalvaie, B.; Johnson, L.; Schroer, J.; Johnston, K. P.; Truskett, T. M. Reversible Self-Assembly of Glutathione-Coated Gold Nanoparticle Clusters via pH-Tunable Interactions. *Langmuir* **2017**, *33*, 12244−12253.
(21) Mosquera, J.; Henriksen-Lacey, M.; García, I.; Martínez-Calvo, M.; Rodríguez, J.; Mascareñas, J. L.; Liz-Marzán, L. M. Cellular Uptake of Gold Nanoparticles Triggered by Host−Guest Interactions. *J. Am. Chem. Soc.* **2018**, *140*, 4469−4472.
(22) Eibling, M. J.; MacDermaid, C. M.; Qian, Z.; Lanci, C. J.; Park, S.-J.; Saven, J. G. Controlling Association and Separation of Gold Nanoparticles with Computationally Designed Zinc-Coordinating Proteins. *J. Am. Chem. Soc.* **2017**, *139*, 17811−17823.
(23) Ho, J.-J.; Ghosh, A.; Zhang, T. O.; Zanni, M. T. Heterogeneous Amyloid B-Sheet Polymorphs Identified on Hydrogen Bond Promoting Surfaces Using 2D SFG Spectroscopy. *J. Phys. Chem. A* **2018**, *122*, 1270−1282.
(24) Kozlowski, R.; Ragupathi, A.; Dyer, R. B. Characterizing the Surface Coverage of Protein−Gold Nanoparticle Bioconjugates. *Bioconjugate Chem.* **2018**, *29*, 2691−2700.
(25) Colangelo, E.; Comenge, J.; Paramelle, D.; Volk, M.; Chen, Q.; Lévy, R. Characterizing Self-Assembled Monolayers on Gold Nanoparticles. *Bioconjugate Chem.* **2017**, *28*, 11−22.
(26) Ong, Q.; Luo, Z.; Stellacci, F. Characterization of Ligand Shell for Mixed-Ligand Coated Gold Nanoparticles. *Acc. Chem. Res.* **2017**, *50*, 1911−1919.
(27) Smith, A. M.; Johnston, K. A.; Crawford, S. E.; Marbella, L. E.; Millstone, J. E. Ligand Density Quantification on Colloidal Inorganic Nanoparticles. *Analyst* **2017**, *142*, 11−29.
(28) Hepel, M.; Tewksbury, E. Ion-Gating Phenomena of Self-Assembling Glutathione Films on Gold Piezoelectrodes. *J. Electroanal. Chem.* **2003**, *552*, 291−305.
(29) Bieri, M.; Bürgi, T. L-Glutathione Chemisorption on Gold and Acid/Base Induced Structural Changes: A PM-IRRAS and Time-Resolved in Situ ATR-IR Spectroscopic Study. *Langmuir* **2005**, *21*, 1354−1363.
(30) Bieri, M.; Bürgi, T. Adsorption Kinetics of L-Glutathione on Gold and Structural Changes During Self-Assembly: An in Situ ATR-IR and QCM Study. *Phys. Chem. Chem. Phys.* **2006**, *8*, 513−520.
(31) Lobo Maza, F.; Méndez De Leo, L.; Rubert, A. A.; Carro, P.; Salvarezza, R. C.; Vericat, C. New Insight into the Interface Chemistry and Stability of Glutathione Self-Assembled Monolayers on Au(111). *J. Phys. Chem. C* **2016**, *120*, 14597−14607.
(32) Vallée, A.; Humblot, V.; Méthivier, C.; Pradier, C.-M. Glutathione Adsorption from UHV to the Liquid Phase at Various pH on Gold and Subsequent Modification of Protein Interaction. *Surf. Interface Anal.* **2008**, *40*, 395−399.
(33) Vallée, A.; Humblot, V.; Méthivier, C.; Pradier, C.-M. Adsorption of a Tripeptide, GSH, on Au (1 1 1) under UHV Conditions; Pm-Rairs and Low T-XPS Characterisation. *Surf. Sci.* **2008**, *602*, 2256−2263.
(34) Donaldson, P. M.; Hamm, P. Gold Nanoparticle Capping Layers: Structure, Dynamics, and Surface Enhancement Measured Using 2D-IR Spectroscopy. *Angew. Chem.* **2013**, *125*, 662−666.
(35) Li, J.; Qian, H.; Chen, H.; Zhao, Z.; Yuan, K.; Chen, G.; Miranda, A.; Guo, X.; Chen, Y.; Zheng, N.; Wong, M. S.; Zheng, J. Two Distinctive Energy Migration Pathways of Monolayer Molecules on Metal Nanoparticle Surfaces. *Nat. Commun.* **2016**, *7*, 10749.
(36) Bian, H.; Li, J.; Chen, H.; Yuan, K.; Wen, X.; Li, Y.; Sun, Z.; Zheng, J. Molecular Conformations and Dynamics on Surfaces of Gold Nanoparticles Probed with Multiple-Mode Multiple-Dimensional Infrared Spectroscopy. *J. Phys. Chem. C* **2012**, *116*, 7913−7924.
(37) Petti, M. K.; Lomont, J. P.; Maj, M.; Zanni, M. T. Two-Dimensional Spectroscopy Is Being Used to Address Core Scientific Questions in Biology and Materials Science. *J. Phys. Chem. B* **2018**, *122*, 1771−1780.
(38) Hamm, P.; Lim, M.; DeGrado, W. F.; Hochstrasser, R. M. The Two-Dimensional IR Nonlinear Spectroscopy of a Cyclic Penta-Peptide in Relation to Its Three-Dimensional Structure. *Proc. Natl. Acad. Sci. U. S. A.* **1999**, *96*, 2036−2041.
(39) Woutersen, S.; Hamm, P. Structure Determination of Trialanine in Water Using Polarization Sensitive Two-Dimensional Vibrational Spectroscopy. *J. Phys. Chem. B* **2000**, *104*, 11316−11320.
(40) Woutersen, S.; Mu, Y.; Stock, G.; Hamm, P. Subpicosecond Conformational Dynamics of Small Peptides Probed by Two-Dimensional Vibrational Spectroscopy. *Proc. Natl. Acad. Sci. U. S. A.* **2001**, *98*, 11254−11258.
(41) Baiz, C. R.; Reppert, M.; Tokmakoff, A. Amide I Two-Dimensional Infrared Spectroscopy: Methods for Visualizing the Vibrational Structure of Large Proteins. *J. Phys. Chem. A* **2013**, *117*, 5955−5961.
(42) Ganim, Z.; Chung, H. S.; Smith, A. W.; DeFlores, L. P.; Jones, K. C.; Tokmakoff, A. Amide I Two-Dimensional Infrared Spectroscopy of Proteins. *Acc. Chem. Res.* **2008**, *41*, 432−441.
(43) Hamm, P.; Lim, M.; Hochstrasser, R. M. Structure of the Amide I Band of Peptides Measured by Femtosecond Nonlinear-Infrared Spectroscopy. *J. Phys. Chem. B* **1998**, *102*, 6123−6138.
(44) Wang, L.; Middleton, C. T.; Singh, S.; Reddy, A. S.; Woys, A. M.; Strasfeld, D. B.; Marek, P.; Raleigh, D. P.; de Pablo, J. J.; Zanni, M. T.; Skinner, J. L. 2DIR Spectroscopy of Human Amylin Fibrils Reflects Stable B-Sheet Structure. *J. Am. Chem. Soc.* **2011**, *133*, 16062−16071.
(45) Hahn, S.; Kim, S.-S.; Lee, C.; Cho, M. Characteristic Two-Dimensional IR Spectroscopic Features of Antiparallel and Parallel B-Sheet Polypeptides: Simulation Studies. *J. Chem. Phys.* **2005**, *123*, 084905.
(46) Moran, S. D.; Zanni, M. T. How to Get Insight into Amyloid Structure and Formation from Infrared Spectroscopy. *J. Phys. Chem. Lett.* **2014**, *5*, 1984−1993.
(47) Lomont, J. P.; Rich, K. L.; Maj, M.; Ho, J.-J.; Ostrander, J. S.; Zanni, M. T. Spectroscopic Signature for Stable B-Amyloid Fibrils Versus B-Sheet-Rich Oligomers. *J. Phys. Chem. B* **2018**, *122*, 144−153.

DOI: 10.1021/acs.jpclett.9b00530
J. Phys. Chem. Lett. 2019, 10, 2481−2486

(48) Evanoff, D. D.; Chumanov, G. Size-Controlled Synthesis of Nanoparticles. 1. "Silver-Only" Aqueous Suspensions Via Hydrogen Reduction. *J. Phys. Chem. B* **2004**, *108*, 13948−13956.
(49) Qian, W.; Krimm, S. Vibrational Analysis of Glutathione. *Biopolymers* **1994**, *34*, 1377−1394.
(50) Rubtsov, I. V. Relaxation-Assisted Two-Dimensional Infrared (RA 2DIR) Method: Accessing Distances over 10 Å and Measuring Bond Connectivity Patterns. *Acc. Chem. Res.* **2009**, *42*, 1385−1394.
(51) Müller-Werkmeister, H. M.; Li, Y.-L.; Lerch, E.-B. W.; Bigourd, D.; Bredenbeck, J. Ultrafast Hopping from Band to Band: Assigning Infrared Spectra Based on Vibrational Energy Transfer. *Angew. Chem., Int. Ed.* **2013**, *52*, 6214−6217.
(52) Cheatum, C. M.; Tokmakoff, A.; Knoester, J. Signatures of B-Sheet Secondary Structures in Linear and Two-Dimensional Infrared Spectroscopy. *J. Chem. Phys.* **2004**, *120*, 8201−8215.
(53) Abramavicius, D.; Zhuang, W.; Mukamel, S. Peptide Secondary Structure Determination by Three-Pulse Coherent Vibrational Spectroscopies: A Simulation Study. *J. Phys. Chem. B* **2004**, *108*, 18034−18045.
(54) Shaw, C. P.; Middleton, D. A.; Volk, M.; Lévy, R. Amyloid-Derived Peptide Forms Self-Assembled Monolayers on Gold Nanoparticle with a Curvature-Dependent B-Sheet Structure. *ACS Nano* **2012**, *6*, 1416−1426.
(55) Kraack, J. P.; Hamm, P. Surface-Sensitive and Surface-Specific Ultrafast Two-Dimensional Vibrational Spectroscopy. *Chem. Rev.* **2017**, *117*, 10623−10664.
(56) Rosenfeld, D. E.; Gengeliczki, Z.; Smith, B. J.; Stack, T.; Fayer, M. Structural Dynamics of a Catalytic Monolayer Probed by Ultrafast 2D IR Vibrational Echoes. *Science* **2011**, *334*, 634−639.
(57) Kwac, K.; Cho, M. Molecular Dynamics Simulation Study of N-Methylacetamide in Water. II. Two-Dimensional Infrared Pump−Probe Spectra. *J. Chem. Phys.* **2003**, *119*, 2256−2263.
(58) Kuroda, D. G.; Vorobyev, D. Y.; Hochstrasser, R. M. Ultrafast Relaxation and 2D IR of the Aqueous Trifluorocarboxylate Ion. *J. Chem. Phys.* **2010**, *132*, 044501.
(59) King, J. T.; Baiz, C. R.; Kubarych, K. J. Solvent-Dependent Spectral Diffusion in a Hydrogen Bonded "Vibrational Aggregate. *J. Phys. Chem. A* **2010**, *114*, 10590−10604.
(60) Kwak, K.; Park, S.; Finkelstein, I. J.; Fayer, M. D. Frequency-Frequency Correlation Functions and Apodization in Two-Dimensional Infrared Vibrational Echo Spectroscopy: A New Approach. *J. Chem. Phys.* **2007**, *127*, 124503.
(61) Adamczyk, K.; Simpson, N.; Greetham, G. M.; Gumiero, A.; Walsh, M. A.; Towrie, M.; Parker, A. W.; Hunt, N. T. Ultrafast Infrared Spectroscopy Reveals Water-Mediated Coherent Dynamics in an Enzyme Active Site. *Chemical Science* **2015**, *6*, 505−516.
(62) Merga, G.; Cass, L. C.; Chipman, D. M.; Meisel, D. Probing Silver Nanoparticles During Catalytic H2 Evolution. *J. Am. Chem. Soc.* **2008**, *130*, 7067−7076.
(63) Greenler, R. G.; Snider, D. R.; Witt, D.; Sorbello, R. S. The Metal-Surface Selection Rule for Infrared Spectra of Molecules Adsorbed on Small Metal Particles. *Surf. Sci.* **1982**, *118*, 415−428.
(64) Edington, S. C.; Gonzalez, A.; Middendorf, T. R.; Halling, D. B.; Aldrich, R. W.; Baiz, C. R. Coordination to Lanthanide Ions Distorts Binding Site Conformation in Calmodulin. *Proc. Natl. Acad. Sci. U. S. A.* **2018**, *115*, E3126−E3134.
(65) Mandal, H. S.; Kraatz, H.-B. Effect of the Surface Curvature on the Secondary Structure of Peptides Adsorbed on Nanoparticles. *J. Am. Chem. Soc.* **2007**, *129*, 6356−6357.
(66) Farrag, M.; Thämer, M.; Tschurl, M.; Bürgi, T.; Heiz, U. Preparation and Spectroscopic Properties of Monolayer-Protected Silver Nanoclusters. *J. Phys. Chem. C* **2012**, *116*, 8034−8043.
(67) di Gregorio, M. C.; Ben Moshe, A.; Tirosh, E.; Galantini, L.; Markovich, G. Chiroptical Study of Plasmon−Molecule Interaction: The Case of Interaction of Glutathione with Silver Nanocubes. *J. Phys. Chem. C* **2015**, *119*, 17111−17116.
(68) Roeters, S. J.; Iyer, A.; Pletikapić, G.; Kogan, V.; Subramaniam, V.; Woutersen, S. Evidence for Intramolecular Antiparallel Beta-Sheet Structure in Alpha-Synuclein Fibrils from a Combination of Two-Dimensional Infrared Spectroscopy and Atomic Force Microscopy. *Sci. Rep.* **2017**, *7*, 41051.
(69) Chuntonov, L.; Haran, G. Maximal Raman Optical Activity in Hybrid Single Molecule-Plasmonic Nanostructures with Multiple Dipolar Resonances. *Nano Lett.* **2013**, *13*, 1285−1290.
(70) Cohn, B.; Engelman, B.; Goldner, A.; Chuntonov, L. Two-Dimensional Infrared Spectroscopy with Local Plasmonic Fields of a Trimer Gap-Antenna Array. *J. Phys. Chem. Lett.* **2018**, *9*, 4596−4601.
(71) Marsh, D. Dichroic Ratios in Polarized Fourier Transform Infrared for Nonaxial Symmetry of Beta-Sheet Structures. *Biophys. J.* **1997**, *72*, 2710−2718.
(72) Stern, S. T.; Adiseshaiah, P. P.; Crist, R. M. Autophagy and Lysosomal Dysfunction as Emerging Mechanisms of Nanomaterial Toxicity. *Part. Fibre Toxicol.* **2012**, *9*, 20.

DOI: 10.1021/acs.jpclett.9b00530
J. Phys. Chem. Lett. 2019, 10, 2481−2486